Journal of Alloys and Compounds 513 (2012) 1–5

Contents lists available at SciVerse ScienceDirect

Journal of Alloys and Compounds

journal homepage: www.elsevier.com/locate/jallcom

Letter

Synthesis and photosensitivity of SnS nanobelts

Hulin Zhang, Chenguo Hu*, Xue Wang, Yi Xi, Xiaoyan Li

Department of Applied Physics, Chongqing University, Chongqing 400044, PR China

ARTICLE INFO

Article history:
Received 24 July 2011
Received in revised form
28 September 2011
Accepted 30 September 2011
Available online 8 October 2011

Keywords:
Stannous sulfide
Semiconductor
Optical sensor

ABSTRACT

One-dimensional stannous sulfide (SnS) nanobelts have been synthesized by molten salt solvent method, with advantages of one-step, low temperature and template-free. The characterization of the nanobelts with X-ray diffraction (XRD), scanning electron microscopy (SEM), transmission electron microscopy (TEM) and selected area electron diffraction (SAED), indicates a single-crystalline orthorhombic structure growing along [0$\bar{1}$2] direction with length up to 6 μm. The electronic valence states of the as-prepared sample are studied by X-ray photoelectron spectrometer (XPS) analysis. The UV–visible–near-infrared reflection spectrum demonstrates the absorption edges of the SnS nanobelts in the short-wave near-infrared region, which could be interpreted in terms of direct transitions from a band gap of 1.33 eV and indirect transitions from a band gap of 1.14 eV. The photoelectric device based on the SnS nanobelts shows distinct optical switching effect under the intermittent illumination of the simulated sunlight with both the rise and decay time less than 300 ms, indicating its great potential applications as optical sensors/switches with a response time in ~ms range.

1. Introduction

Recent investigations on nanostructures of metallic sulfides such as CdS, CuS, ZnS have attracted considerable interest owing to their application in optical and electronic devices [1–3]. Among these materials binary tin sulfides (SnS, SnS_2, Sn_2S_3, Sn_3S_4, Sn_4S_5) are known of which SnS and SnS_2 are significantly important because of their interesting properties and potential technological applications [4–6]. SnS is a p-type semiconductor with layered orthorhombic crystal structure. The orthorhombic herzenbergite modification of SnS consists of double layers perpendicular to *c*-axis in which Sn and S atoms are tightly bound. The direct and indirect band gap of SnS were reported to be 1.2–1.5 and 1.0–1.2 eV, respectively [7]. The narrow band gap and the interesting structural property of SnS make it a potential candidate for solar absorber in thin film solar cells, semiconductor sensors and holographic registrar systems [8–11]. Besides, semiconductor sulfides with 1D belt-like morphology, which can maximize surface-to-volume ratio and shorten the carrier transit time [12], are more attractive for possible applications in nanoscale devices [13]. Nevertheless, photosensitive devices based on 1D SnS nanobelts have seldom been reported for photodetector applications.

Because of the above wide application, the synthesis of SnS nanobelts has been attracting considerable attention. Qian's group has developed a multi-step wet chemical route to synthesize SnS nanobelts [13]. Liu and Xue [14] also reported poly vinyl pyrrolidone (PVP) assisted solvothermal method for synthesizing SnS nanobelts. Still, a facile, environmentally friendly and cost-effective method without using surfactant for the preparation of SnS nanobelts with high quality under ambient pressure and at low temperature is a goal of many researchers.

Herein, we take a new strategy to prepare SnS nanobelts by a low temperature molten salt solvent method that is based on chemical reactions in eutectic composite salt melts at temperature of 200 °C in the absence of organic dispersant or capping agents. The as-produced SnS nanobelts are characterized by XRD, SEM, TEM and XPS. The UV–visible–near infrared reflection spectrum is studied. In addition, the photoelectric device is fabricated from SnS nanobelts. The photoelectric properties of the device have been investigated under the irradiation of the simulated sunlight. The photocurrent change with incidence illumination intensity is also examined.

2. Experimental

All of the analytically pure chemical reagents including $LiNO_3$, KNO_3, $SnCl_2{\cdot}2H_2O$, $N_2H_4{\cdot}H_2O$ (hydrazine hydrate) and $(NH_2)_2CS$ (thiourea) were purchased from Chongqing Chemical Company and used as received without further purification. 6 g of mixed ($LiNO_3/KNO_3$ = 1/2) was put in a 25 mL Teflon-lined autoclave, and 0.1 mmol $SnCl_2{\cdot}2H_2O$, 0.1 mmol thiourea and 5 mL hydrazine hydrate were added into the mixed nitrates. The vessel was sealed and then kept at 200 °C for 24 h, and then let cool down naturally. The products were washed with deionized water and absolute ethanol, and then dried at 60 °C for 2 h. The products were characterized by XRD (BDX3200, China), SEM (TESCAN VEGA II) and TEM (TEM, JEOL4000EX). X-ray photoelectron spectrometer (XPS) analysis was performed on an ESCALab MKII using Mg Ka as the exciting source. An UV–vis–NIR spectrophotometer (Hitachi U-4100) was used to investigate the optical properties of the synthesized products.

* Corresponding author. Tel.: +86 23 65678362; fax: +86 23 65678362.
E-mail addresses: hucg@cqu.edu.cn, hu_chenguo@yahoo.com (C. Hu).

0925-8388/$ – see front matter © 2011 Elsevier B.V. All rights reserved.
doi:10.1016/j.jallcom.2011.09.096

To investigate the photosensitive property of the obtained SnS nanostructures, a photoelectric device was fabricated with three facile steps. The first is to obtain a SnS nanobelt film by pressing SnS nanobelts under the pressure of 10 MPa. The second is to ultrasonically clean two pieces of conductive glasses (FTO) with detergent solution and deionized water several times to remove oil, grease, and dust on the surface. The last is to encapsulate the sandwich structure with epoxy resin to fabricate a photodetector device. The photoelectronic performance of the device was investigated under the irradiation of simulated sunlight (CHF-XM-500W), and the photocurrent was recorded using a computerized data acquisition system equipped with a source meter (KEITHLEY 2400).

3. Results and discussion

Typical XRD pattern of the product is shown in Fig. 1a. The product can be perfectly indexed to the orthorhombic phase of the SnS with the lattice constants of $a = 4.33$ Å, $b = 11.19$ Å, $c = 3.98$ Å (JCPDS 39-0354) and no peaks of other phases are detected. Fig. 1b shows the energy dispersive X-ray spectrum (EDS) of the sample, which confirms the composition of tin and sulfur. The C and Si signals come from the substrate.

SEM and TEM were employed to characterize the morphology, size and crystal structure of the SnS sample. SEM image in Fig. 2a illustrates a nanobelt-like morphology of the synthesized nanocrystals. The width of nanobelts is ranging from 50 to 200 nm and the length is up to 6 μm, as is shown by the TEM image in Fig. 2b. Fig. 2c and d gives the TEM image of a single SnS nanobelt and its SEAD pattern, respectively, which suggest that the SnS nanobelts are single-crystalline and grow along [0$\bar{1}$2] direction.

To investigate the growth process of the SnS nanobelts, the time-dependent and temperature-dependent experiments were carried out, indicating that the reaction time cannot obviously change the morphology and size of the products at the temperature of 200 °C and no products are obtained with the reaction temperature below 180 °C. (We compare the obtained products with different reaction time of 24 h, 36 h and 48 h and at different reaction temperature

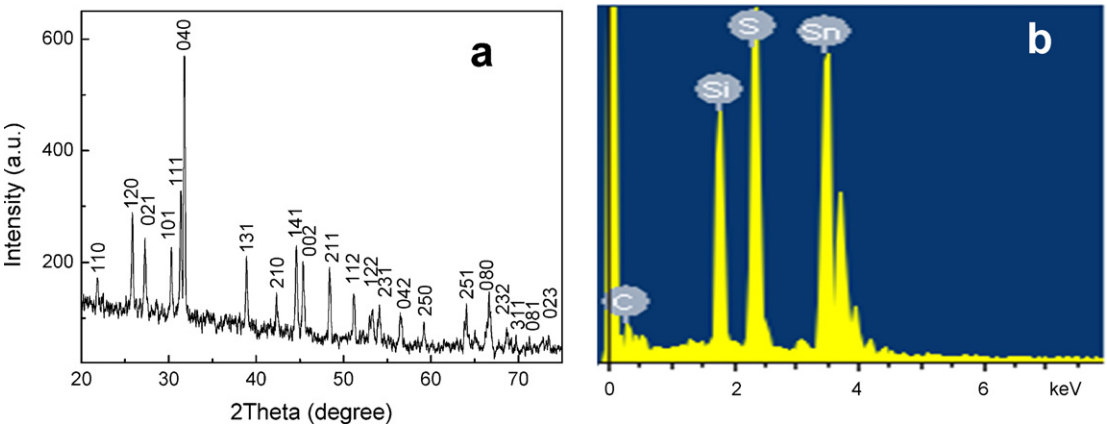

Fig. 1. XRD pattern (a) and the energy dispersive X-ray spectrum (b) of the SnS nanobelts obtained by molten salt solvent method.

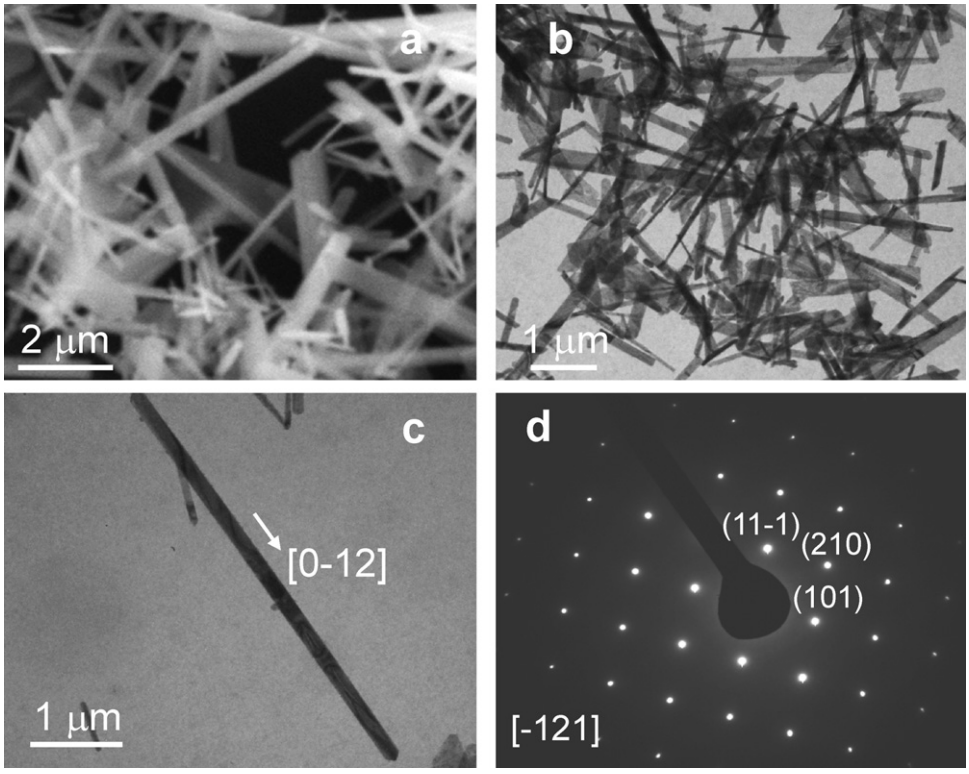

Fig. 2. SEM image (a) and TEM image (d) of the SnS nanobelts, TEM image (c) of a single SnS nanobelt and selected area electron diffraction pattern (d).

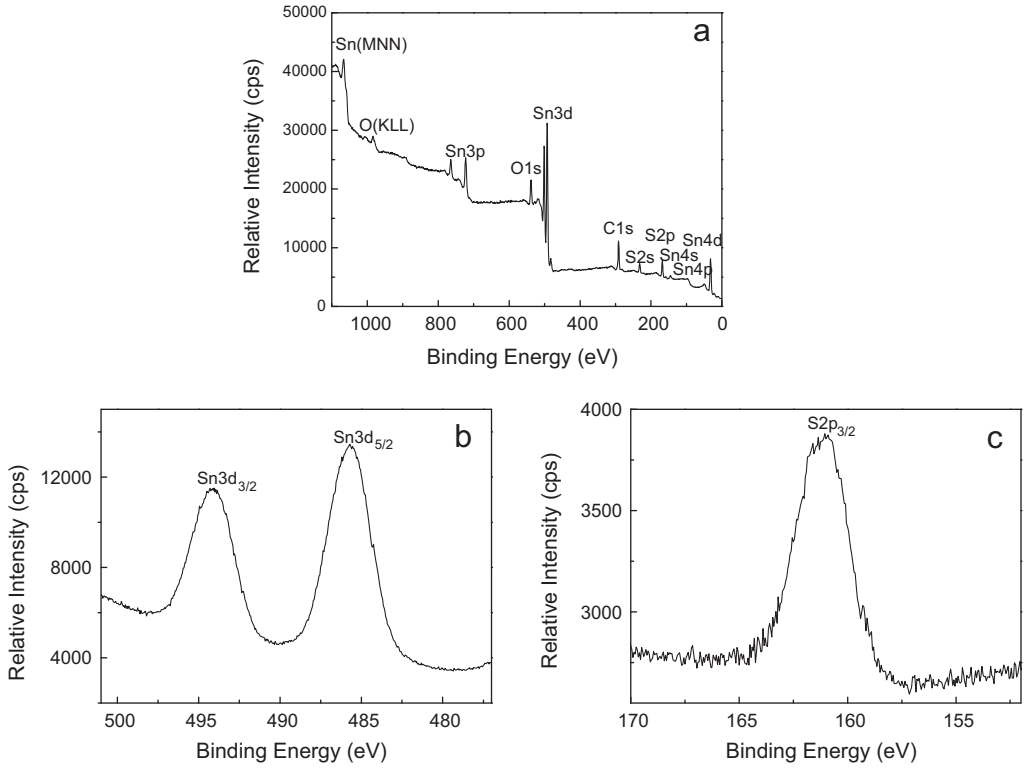

Fig. 3. XPS spectra of SnS products: a typical survey spectrum (a), Sn 3d core level (b), S 2p core level (c).

of 150 °C, 180 °C and 200 °C.) Furthermore, we find that hydrazine hydrate plays an important role in the experiment. On the one hand, hydrazine hydrate as a reducing agent can provide a reducing environment to prevent Sn^{2+} from being oxidized. On the other hand, hydrazine hydrate as a chelating agent can control the growth and direct the structure-formation of crystals due to the selective absorption of molecules and ions in reaction mixture on different crystal faces [15].

In above synthetic systems, the chemical reactions can be expressed as the following equations:

$$SnCl_2 + N_2H_4 \rightarrow [Sn(N_2H_4)_3]^{2+} + 2Cl^-$$

$$(NH_2)_2CS + H_2O \rightarrow (NH_2)_2CO + S^{2-} + 2H^+$$

$$[Sn(N_2H_4)_3]^{2+} + S^{2-} \rightarrow SnS\downarrow + 3N_2H_4$$

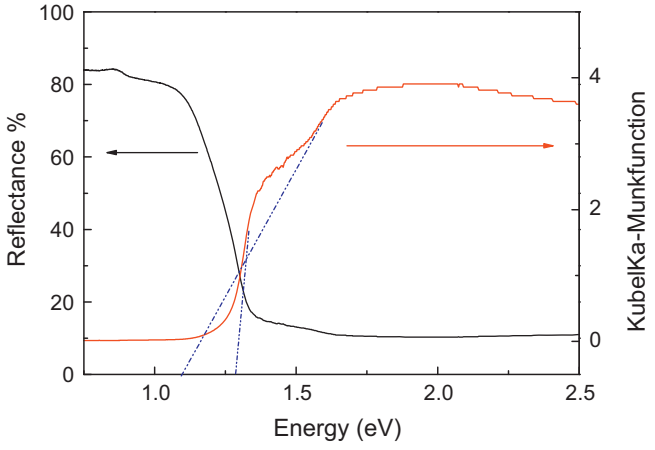

Fig. 4. UV–visible–NIR reflection spectrum and Kubelka–Munk function of the SnS nanobelts.

Stannous chlorides will firstly dissociate to release metal ions which then react with hydrazine to form the relatively stable metal ions complex [16]. Secondly, the S^{2-} is produced from thiourea through hydrolysis reaction with increasing the reaction temperature. Finally, the S^{2-} may attack the metal ions of the complex, as causes the bonds between the metal ions and the N atoms of hydrazine to become weaker and the bonds between the metal ions and S^{2-} to form little by little [17], resulting in the formation of the SnS nanocrystals.

The purity and composition of the as-prepared sample are studied by XPS analysis. The XPS spectra of the product are shown in Fig. 3. Fig. 3b and c shows the photoelectron spectrum of Sn 3d core

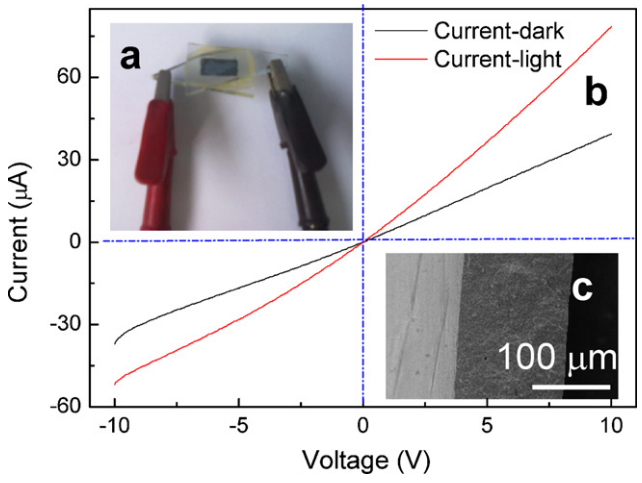

Fig. 5. The photograph of the device (a), *I–V* curves (b) of the photoelectronic device based on SnS nanobelt film in the dark (solid line) and under the simulated sunlight (dashed line) with intensity of 78 mW/cm^2 and SEM image of the film in side view (c).

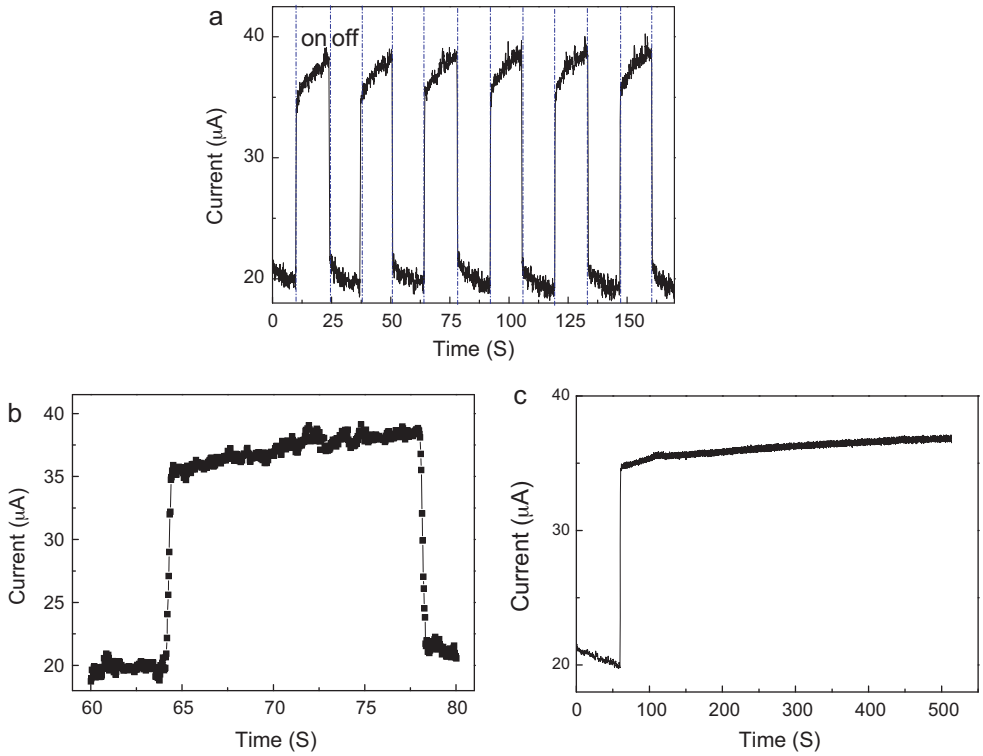

Fig. 6. Photocurrent responses to switching of light at a bias of 5 V under the simulated sunlight with intensity of 78 mW/cm^2 (a), the enlarged one response under the simulated sunlight (b) and current-time response at a bias of 5 V under the simulated sunlight with intensity of 78 mW/cm^2 (c).

level and S 2p core level, respectively. The peak at 485.7 eV corresponds to the binding energy of Sn $3d_{5/2}$ and the corresponding binding energy of S $2p_{3/2}$ is 161.2 eV. The results are in agreement with the reported data [18]. The ratio of integral area for S 2p to Sn $3d_{5/2}$ is about 1:1.08, which coincides with the results of XRD. No evidence of Sn^{4+} (binding energy at 485.9 eV) is detected in the spectra.

In order to investigate the optical property of the SnS nanobelts, the diffuse reflectance spectrum is performed by casting the dispersed SnS nanobelts on a glass substrate. The diffuse reflectance spectrum and Kubelka–Munk function of the SnS nanocrystals are shown in Fig. 4. The energy gap of SnS nanobelts can be estimated by extrapolating the linear part of Kubelka–Munk function, which is the ratio between the absorption and scattering factor from the optical diffuse reflectance spectrum [19,20]. Obviously, the Kubelka–Munk function in Fig. 4 shows two band gaps, 1.33 and 1.14 eV, which is direct band gap and indirect band gap according to previous literatures [7,21], respectively.

To explore the photoelectric property of the SnS crystals, a photoelectric device was fabricated in the sandwich structure. The photograph of the device based on the SnS nanobelts is shown in the inset of Fig. 5a. It is seen under SEM the thickness of the nanobelt film is around 120 μm (Fig. 5c) and the effective acreage is around 0.6 cm^2. Typical *I–V* curves of the SnS nanobelt device in the dark (solid line) and under the simulated sunlight (dashed line) with intensity of 78 mW/cm^2 are shown in Fig. 5b in scanning voltage ranging from −10 V to +10 V. The current under illumination is much larger than that in the dark, and both curves in the dark and under illumination present almost linear characteristic.

The photocurrent response of the device is performed at a bias of 5 V under the simulated sunlight with intensity of 78 mW/cm^2. The reversible photocurrent switching effect of the device is obviously displayed in Fig. 6a when the simulated sunlight is periodically switched on and off. In order to estimate the response time of rise and decay of the current, one response cycle is magnified. Fig. 6b shows a single time-response cycle. In our experiment, every measuring interval of KEITHLEY 2400 is represented by the equal intervals of 30 ms. It is clear that both the rise and decay time is less than 300 ms, with current change of more than 15 μA in exposure to the simulated sunlight with intensity of 78 mW/cm^2. Obviously, the response sensitivity is acceptable in most of the applications of photodetectors [22].

As a photoelectric device, the stability is significantly of importance. Fig. 6a shows the photocurrent stability of the device at 5 V bias over a 500 s interval in exposure to the simulated sunlight with intensity of 78 mW/cm^2, indicating the stability of the photocurrent with charging effect modulating the magnitude of the current response within ±7%. The good stability can be attributed to the sandwich structure of the device which can prevent the SnS nanobelt film from influence by the air ambient, the change in gaseous atmosphere or humidity that can greatly affect the photocurrent [23,24].

It is an important advantage of powder photoelectric materials that flexible photoelectric devices can be obtained by the printing technology as the powder of nanomaterials can easily form the thin film on flexible substrates. In addition, the nanobelt films have a higher conductivity in comparison with the corresponding nanoparticle films due to the network structure formed by the nanobelts. Although the conductivity of our SnS nanobelt films might be lower than that of the continuous films prepared by the magnetic sputtering coating or chemical vapor deposition, the light absorption ability of the nanobelt films is higher than that of the continuous films due to the vast surface microstructures. On the other hand, as the SnS nanobelts can be cost-effectively synthesized by the facile molten salt method, the photoelectric devices based on the SnS nanobelt film with the various shapes and sizes can be achieved on a large scale.

4. Conclusions

SnS nanobelts have been synthesized by the molten salt solvent method. This approach is novel, one-step, low temperature, cost effective and mass-producible. A photoelectric device has been fabricated simply from the SnS nanobelts. Our investigation demonstrates that the SnS nanobelts can be used in optical sensors/switches.

Acknowledgments

This work is supported by the NSFC (60976055), Project (WLYJS-BJRCTD201101) of the Innovative Talent Funds for 985 Project, and Postgraduates' Innovative Training Project (S-09109) of the 3rd-211 Project, and the large-scale equipment sharing fund of Chongqing University.

References

[1] J.R. Lakowicz, I. Gryczynski, G. Piszczek, C.J. Murphy, J. Phys. Chem. B 106 (2002) 5365–5370.
[2] M. Xin, K.W. Li, H. Wang, Appl. Surf. Sci. 256 (2009) 1436–1442.
[3] J.H. He, Y.Y. Zhang, J. Liu, D. Moore, G. Bao, Z.L. Wang, J. Phys. Chem. C 111 (2007) 12152–12156.
[4] Z.J. Wang, S.C. Qu, X.B. Zeng, J.P. Liu, C.S. Zhang, F.R. Tan, L. Jin, Z.G. Wang, J. Alloys Compd. 482 (2009) 203–207.
[5] T. Jiang, G.A. Ozin, J. Mater. Chem. 8 (1998) 1099–1108.
[6] V. Piacente, S. Foglia, P. Scardala, J. Alloys Compd. 177 (1991) 17–30.
[7] J.B. Johnson, H. Jones, B.S. Latham, J.D. Parker, R. Engelken, C. Barber, Semicond. Sci. Technol. 14 (1999) 501–507.
[8] M. Gunasekaran, M. Ichimura, Sol. Energy Mater. Sol. Cells 91 (2007) 774–778.
[9] B. Ghosh, M. Das, P. Banerjee, S. Das, Semicond. Sci. Technol. 24 (2009) 025024 (7 pp.).
[10] T. Jiang, A.G. Ozin, A. Verma, R.L. Bedard, J. Mater. Chem. 8 (1998) 1649–1656.
[11] M. Radot, Rev. Phys. Appl. 18 (1977) 345–351.
[12] P.C. Wu, Y. Dai, T. Sun, Y. Ye, H. Meng, X.L. Fang, B. Yu, L. Dai, ACS Appl. Mater. Interfaces 3 (2011) 1859–1864.
[13] C.G.K. An, B. Tang, G.Z. Shen, C.R. Wang, Q. Yang, B. Hai, Y.T. Qian, J. Cryst. Growth 244 (2002) 333–338.
[14] J. Liu, D.F. Xue, Electrochim. Acta 56 (2010) 243–250.
[15] M.J. Manos, M.G. Kanatzidis, Inorg. Chem. 48 (2009) 4658–4660.
[16] Y.D. Li, C.W. Li, H.R. Wang, L.Q. Li, Y.T. Qian, Mater. Chem. Phys. 59 (1999) 88.
[17] Y.D. Li, M. Sui, Y. Ding, G.H. Zhang, J. Zhuang, C. Wang, Adv. Mater. 12 (2000) 818.
[18] H.L. Su, Y. Xie, Y.J. Xiong, P. Gao, Y.T. Qian, J. Solid State Chem. 161 (2001) 190–196.
[19] W.M. Wesley, G.H.H. Wendlandt, Reflectance Spectroscopy, Interscience Publishers, John Wiley, New York, 1966.
[20] J. Li, Z. Chen, X.X. Wang, D.M. Proserpio, J. Alloys Compd. 262 (1997) 28–33.
[21] E. Guneria, C. Ulutasb, F. Kirmizigulb, G. Altindemirb, F. Godec, C. Gumusb, Appl. Surf. Sci. 257 (2010) 1189–1195.
[22] M.T.S. Nair, P.K. Nair, R.A. Zingaro, E.A. Meyers, J. Appl. Phys. 74 (1993) 1879–1884.
[23] Y.S. Tian, C.G. Hu, X.S. He, C.L. Cao, G.S. Huang, K.Y. Zhang, Sens. Actuators B: Chem. 144 (2010) 203–207.
[24] J. Nelson, A.M. Eppler, I.M. Ballard, J. Photochem. Photobiol. A: Chem. 148 (2002) 25–31.